Boundary-Layer Meteorol (2013) 147:103–121
DOI 10.1007/s10546-012-9780-z

ARTICLE

Measurements of Turbulence and Dispersion in Three Idealized Urban Canopies with Different Aspect Ratios and Comparisons with a Gaussian Plume Model

Pablo Huq · Pasquale Franzese

Received: 30 June 2011 / Accepted: 11 October 2012 / Published online: 2 November 2012

Abstract Water-tunnel measurements of velocity, turbulence and scalar concentration for three model urban canopies with aspect ratios A_r of building height-to-width of 0.25, 1 and 3 are presented. The measurements for the canopies with $A_r = 1$ and 3 are new, while the measurements for $A_r = 0.25$ were previously published. A passive scalar was continuously released from a near-ground point source, and the concentration was measured at several distances from the source and at different heights above the ground. Plume spreads, concentration and distance from the source were non-dimensionalized using length, time and velocity scales reflecting the geometry of the buildings. The scaling collapses the data for all aspect ratios and is valid when the vertical extent of the plume is smaller than the canopy height. The observed plume spreads are compared with analytical relations, which predict linear growth in both transverse and vertical directions. The observed mean concentration is compared with a Gaussian dispersion model that predicts a -2 power-law decay with distance from the source.

Keywords Dispersion length scales · Gaussian plume model · Obstacle arrays · Urban canopy · Urban dispersion experiments · Water tunnel

1 Introduction

The interaction of atmospheric flow with the buildings of an urban area generates a boundary layer with specific characteristics. A major difference compared to boundary layers over flat terrain (Schlichting 1968) is the large size of the roughness elements (i.e. the buildings) that are of the order of the overall boundary-layer height. The vertical structure of the urban

P. Huq
College of Earth, Ocean and Environment, University of Delaware, Newark, DE 19716, USA
e-mail: huq@udel.edu

P. Franzese (✉)
Ecology and Environment, Inc., Lancaster, NY 14086, USA
e-mail: pfranzese@ene.com

boundary layer comprises a roughness sublayer near the ground and an inertial sublayer above. In the lowest part of the roughness sublayer, the buildings form an urban canopy layer. The large roughness of the urban boundary layer attenuates wind speeds, and the large transfers of energy, humidity and radiant fluxes can affect the urban weather (Collier 2006). This raises concern about the dispersion patterns and fate of contaminants released in urban areas (Oke 1987; Molina and Molina 2004). Urban canopy parametrizations have been developed for numerical models to simulate the dynamic effects of buildings (Chin et al. 2005; Delle Monache et al. 2009). However, generalization is difficult as turbulence characteristics depend upon local building arrangements and geometry.

Roth (2000) presented a comprehensive review of atmospheric turbulence data over cities including vertical profiles of friction velocity u_*, turbulence length scales, velocity and scalar spectra, and root-mean-square (r.m.s., or standard deviation) of alongwind, transverse and vertical velocity fluctuations σ_u, σ_v and σ_w, respectively. Turbulence intensities σ_u/U and σ_w/U, where U is the local mean velocity, attained values of about 0.6 and 0.3 close to the ground, with the results most scattered for nighttime conditions. The consensus of field investigations undertaken in European cities such as Zurich (Rotach 1995), Basel (Rotach et al. 2005), Marseille (Grimmond et al. 2004; Mestayer et al. 2005) and London (Dobre et al. 2005) is of augmented turbulent velocity variances compared to flat rural terrain. Data within the urban canopy (i.e. between the ground and the rooftop level) at Oklahoma City and midtown New York City (Manhattan) have been reported by Hanna et al. (2007). The urban canopy at Manhattan includes deep urban canyons (the urban canyon is defined as the space between the buildings in the direction of the mean wind.)

Meteorological data in the boundary layer over urban areas are more scarce than over rural sites, and methods to estimate urban meteorological variables using measurements from rural sites were presented by Luhar et al. (2006). Alternative forms of investigation can be useful to mitigate the costs of urban data collection. For example, the MUST (Mock Urban Setting Test) field experiment (Biltoft 2001) has been undertaken using a large-scale model of an urban canopy, where the roughness elements were formed by arrays of shipping containers. The control and repeatability of laboratory experiments is also attractive. Macdonald et al. (1998) undertook wind-tunnel experiments to develop parametrizations of surface roughness due to obstacle arrays in terms of frontal and plan area densities λ_f and λ_p. Macdonald (2000) found that the mean velocity within the urban canopy could be modelled by the rooftop velocity and an exponential decay factor, and noted that skimming flow occurred for $\lambda_f > 0.2$; neutral flow above the roughness elements was described by a logarithmic-law profile. Cheng and Castro (2002) and Castro et al. (2006) determined spatially-averaged mean velocity profiles from hot-wire and laser Doppler anemometry within the roughness sublayer of cubic elements in a wind tunnel, and Gailis and Hill (2006) resolved velocities and scalar concentration in a wind-tunnel simulation of MUST data, and noted channelling of the plume in the direction of the mean wind. Yee et al. (2006) compared the MUST wind-tunnel data with water-tunnel simulations and found qualitatively similar results. The MUST experimental data were also extensively analyzed using computational fluid dynamics simulations (e.g., Milliez and Carissimo 2007). Direct numerical simulations of model urban canopies have been performed by Coceal et al. (2006), who showed the unsteady nature of the canopy flow, and the effects of building layout on space- and time- averaged turbulence statistics.

A measure of the interaction between the buildings and the flow is given by the porosity of the urban canopy, which determines the proportion of flow channelling through the gaps between the buildings, and flow around and above the area. Porosity depends on the geometry and the arrangement of the buildings, and can be estimated by several quantities, including λ_f, λ_p, and the aspect ratio of building height H to building width w_b, $A_r = H/w_b$. Thus

parametrization of an urban canopy flow requires at least both areal parameters as well as building scales. For instance, the drag exerted by the canopy is strongly influenced by the area density factors, whereas flow channelling is affected by A_r. Values of aspect ratios in the urban environment typically range between 0.1 and 3 (Grimmond and Oke 1999; Macdonald et al. 1998), while industrial areas can have $A_r \approx 0.25$: for Oklahoma City and Salt Lake City $A_r \approx 1$, and for Manhattan (NYC) $A_r \approx 3$.

We present measurements of turbulence, velocity and concentration of material released from a continuous point source for three model urban canopies with aspect ratios $A_r = 0.25$, 1 and 3. The measurements for the canopy with $A_r = 0.25$ were taken by Macdonald and Ejim (2002) to reproduce the set-up of the MUST experiment, which consisted of a regular series of prisms. The measurements for the canopies with $A_r = 1$ (arrays of cubes) and $A_r = 3$ (arrays of tall prisms) are new. All experiments simulate in-canopy dispersion in the near field, where the plume vertical dimension is smaller or comparable to the mean building height.

When the vertical dimension of the plume is larger than the canopy height, dispersion is governed by the scales of the background atmospheric boundary layer (Franzese and Huq 2011). When the plume is below the canopy height, we will show that dispersion is controlled by canopy parameters. Prediction of dispersion requires knowledge of the time and length scales of turbulence. We identify the vertical turbulence length scale as the height of the canopy, and the transverse length scale as one half of the gap between the buildings. The transverse and vertical turbulence time scales are defined by the ratio of the respective length scale to r.m.s. velocity. The concentration data from the three experiments are scaled in order to collapse and to be compared with an analytical urban dispersion model.

Section 2 describes the experimental set-up, and Sect. 3 summarizes the dispersion model equations. Section 4 discusses measurements of profiles of mean and turbulent velocity fields, while plume spreading and concentration data are discussed and compared with the model predictions in Sect. 5. Conclusions follow in Sect. 6.

2 Experimental Methods

Experiments for the smallest aspect ratio canopy with $A_r = 0.25$ were undertaken in a water tunnel at the University of Waterloo by Macdonald and Ejim (2002). The tunnel is 12.8 m long with a 1.2 m × 1.2 m × 2.4 m long test section, and the canopy comprises 10 rows of four buildings each. Each model building has height $H = 50$ mm, width $w_b = 0.2$ m, and length in the alongwind direction $B = 50$ mm. The lateral spacing $G = 0.1$ m and the longitudinal spacing $S = 0.2$ m. The plan area density $\lambda_p = Bw_b/[(w_b+G)(B+S)]$ and the frontal area density $\lambda_f = Hw_b/[(w_b+G)(B+S)] = 0.13$. Turbulent velocity measurements were made with a micro-acoustic Doppler velocimeter. The scalar was hot water released at mid-height of the buildings; scalar measurements were made with resistance temperature detectors at the downwind distances $x/B = 2.6, 7.6, 12.6, 17.6$ and 22.6. Details of the experimental facilities, flow, turbulence and concentration measurements are available in Macdonald and Ejim (2002).

Laboratory measurements for the $A_r = 1$ and 3 canopies were undertaken in a water tunnel at the Environmental Fluids Laboratory at the University of Delaware. The water tunnel is 4 m long, 0.4 m deep, and 0.25 m wide. The Plexiglas walls enable flow visualization techniques, and a free surface allows measurements with micro-conductivity probes. The free surface affects the pressure gradient near the top of the water column and data were not obtained in this region. Two uniform canopies with $H = 32$ mm and $H = 96$ mm, and $w_b = 32$ mm

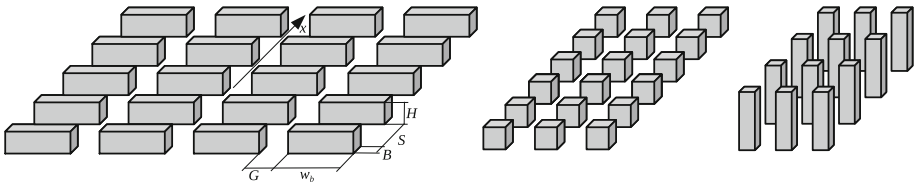

Fig. 1 Schematic of the model urban canopies with $A_r = 0.25$ (*left panel*), $A_r = 1$ (*centre panel*), and $A_r = 3$ (*right panel*). H is the building height, B is the length of the building along the x-axis, w_b is the building width, G and S are lateral and longitudinal spacings between buildings, respectively

were utilized for the experiments. The canopies consist of 22 rows of three 32-mm square buildings, with lateral spacing $G = 35\,\text{mm}$ and longitudinal spacing $S = 50\,\text{mm}$. The area density factors are $\lambda_p = \lambda_f = 0.19$ for the $A_r = 1$ canopy; $\lambda_p = 0.19$ and $\lambda_f = 0.56$ for the $A_r = 3$ canopy. Figure 1 shows a schematic of the three configurations, and the geometry of the canopy.

Velocity measurements were taken along the centreline of an urban canyon in the x-z plane, where x and z indicate the alongwind and the vertical directions, respectively. Scalar measurements were taken at five distances downwind of the source along the centreline of the urban canyon in the x-z plane, and in the lateral y direction at the ground.

Velocity measurements were determined using particle image velocimetry (PIV) with particles of diameter 75 μm and a 5-mm thick light sheet. Mean velocity U, r.m.s. alongwind and vertical velocity σ_u and σ_w, and Reynolds stress $-\overline{uw}$ were determined at a distance $x/B = 38$ from the source from 60-s long time series recorded on video. The errors from measurement uncertainty are ±1 % for U, ±5 % for σ_u and σ_w, ±15 % for $\overline{uw}$. For the urban canopy flow an order of magnitude estimate of the large-eddy turnover time is w_b/U_b or H/U_b, where U_b is the flow velocity at the building height. Since turnover time ranges from 0.4 to 1.2 s, a 60-s time series includes approximately 50–100 large-eddy turnover realizations, and is sufficient for stable values of variance and mean of turbulent quantities. The water tunnel is operated with a steady freestream velocity $U_\infty = 94\,\text{mm s}^{-1}$ for $A_r = 1$ and $110\,\text{mm s}^{-1}$ for $A_r = 3$. A Counihan vortex generator comprising 0.1-m high vorticity generators was used to accelerate development of the boundary layer (Counihan 1969). The vorticity generators are elliptic and positioned at alternating angles of 5° to the direction of the mean flow; this results in a flow where velocity is transversely uniform to within 1 % in the working section outside of the sidewall boundary layers (for details, see Cheah et al. 1983).

Boundary layers form at the walls of wind and water tunnels. Thus the scale of an experiment is a compromise between reducing the size of the canopy to increase the distance from the walls, and enlarging the size of the canopy to increase the Reynolds number. The distance between the buildings and the sidewall is 42 mm, whereas the boundary layers in the experiments grow to a thickness of 10 mm far downwind. As a precaution no measurements were taken within 42 mm of the sidewalls, and there are no discernible boundary-layer effects in the canyon where measurements were taken. Experiments were repeated four times so as to check repeatability. The errors from repeatability over four realizations, estimated for each variable as the average over all data points, are ±3 % for U, ±10 % for σ_u and σ_w, and ±25 % for $\overline{uw}$.

The scalar source is a pipe of diameter 2 mm. A neutrally buoyant solution of alcohol and brine is pumped through the pipe at a rate of $1{,}400\,\text{mm}^3\text{s}^{-1}$, maintained by a flow meter. The pipe exit is located at the fifth row to ensure discharge into fully developed canopy flow. The

source is at ground level ($z = 0$), at the centreline of the canyon ($y = 0$), at the centre of the row ($x = 0$). The source momentum flux results in a potential core (i.e. the region near the source where the jet has constant width) whose length depends on the exit velocity and stratification (Rajaratnam 1976, Fig. 6. 17 and Huq 1997, Fig. 11). The length of the potential core in the experiments is of the order of 10 source diameters, and therefore a virtual origin at $x/B = 1$ was used to model the source location.

Concentration is measured by a micro-conductivity probe with spatial resolution of 0.4 mm and temporal resolution of 100 Hz. The dynamic range is more than three decades, as the probe is capable of detecting concentrations below 0.1 % of the concentration at the source. Transverse and vertical concentration profiles are taken at the non-dimensional distances $x/B = 2.3$, 4.8, 7.5, 13 and 17.8 downwind of the source. The Schmidt number ν/κ, where ν is the kinematic viscosity and κ is the scalar diffusivity, is approximately 700. At the scales under investigation, dispersion is driven by turbulence, and molecular diffusion has a negligible effect, both in the water tunnel and in the atmosphere. Since the relationship between concentration and voltage is linear over the small range of concentrations used in the experiments, the concentration is given by $c/C_\mathrm{o} = (V - V_\mathrm{b})/(V_\mathrm{o} - V_\mathrm{b})$, where c/C_o is the instantaneous fraction of the source concentration C_o, V is the instantaneous voltage signal, V_b is the background voltage in the water tunnel, and V_o is the voltage in the source solution. The fluctuating signal is recorded on a computer using an analogue-to-digital (A–D) converting board. The conductivity probe is mounted to a traversing rig moving in the transverse, longitudinal, and vertical directions to accuracy higher than 0.5 mm. The estimated errors for mean concentration are ±1 % from instrument uncertainty and ±10 % from repeatability.

For the $A_r = 0.25$ canopy, the Reynolds number $Re_\mathrm{H} = U_\mathrm{H} H/\nu$ based on building height and wind speed at that height is about 2,500 (taking $\nu = 1\,\mathrm{mm^2\,s^{-1}}$ for water). For the $A_r = 1$ canopy $Re_\mathrm{H} = 1,664$, and for the $A_r = 3$ canopy $Re_\mathrm{H} = 7,400$. While higher Reynolds numbers are certainly desirable, such low values are common in water-tunnel and wind-tunnel experiments. For instance, $Re_\mathrm{H} = 2,020$ in Yee et al. (2006), and $Re_\mathrm{H} = 2,859$ in Cheng and Castro (2002).

An early estimate of the critical Reynolds number as $Re_\mathrm{H} \approx 10^4$, determined from the experiments of Golden (1961), is generally considered very conservative (Snyder 1981, p. 135). Using more accurate measurements, Castro and Robins (1977) observed Reynolds number independence in a shear flow when $Re_H > 4{,}000$ (Snyder 1981, p. 136). More recently, Cheng and Castro (2002) found that the drag coefficient is only weakly dependent on the Reynolds number for $Re_H \geqslant 1191$. (Re_H in Cheng and Castro, 2002, can be calculated from their Table 1 as $Re_\mathrm{H} = Re\sqrt{(C_\mathrm{D})_{U_\infty}/(C_\mathrm{D})_{U_\mathrm{H}}}$). Also, the systematic study of the critical roughness Reynolds number $Re_* = u_* z_\mathrm{o}/\nu$ for rough-wall boundary layers conducted by Snyder and Castro (2002) shows that the critical $Re_* = 1$ in a staggered array of flat plates, and is possibly lower for more closely spaced elements. In our $A_r = 1$ canopy $Re_* \approx 20$, assuming $z_\mathrm{o} \approx 0.15H$ (Hanna et al. 2003).

3 Gaussian Dispersion Model

We use the Gaussian plume model presented by Franzese and Huq (2011), which was applied to study dispersion above the canopies of four cities. The mean concentration field c of a tracer emitted from a ground-level continuous source is approximated by the reflected Gaussian relation

Table 1 Summary of experimental data and model parameters, including: building height H; building width w_b; source size $\sigma_o = \sigma_{yo} = \sigma_{zo}$; freestream velocity U_∞; vertical and transverse r.m.s. velocity σ_w and σ_v; vertical and transverse turbulence time scales T_z and T_y; vertical and transverse turbulence length scales L_z and L_y; rooftop-level wind speed U_b; advection speed U used in Eq. 1; and the ratio U/U_b

A_r	Q (mm^{3}s^{-1})	σ_o (mm)	H (mm)	U_∞ (mm s^{-1})	σ_w (mm s^{-1})	σ_v (mm s^{-1})	T_z (s)	T_y (s)	L_z (mm)	L_y (mm)	U_b (mm s^{-1})	U (mm s^{-1})	U/U_b
0.25	2180	5	50	78	4.7	7.0	10.7	7.1	50	50.0	52	52	1.00
1.00	1400	2	32	94	2.1	3.1	15.5	5.6	32	17.5	52	27	0.52
3.00	1400	2	96	110	1.5	2.2	64.3	7.8	96	17.5	77	28	0.36

$$c = \frac{Q}{\pi U \sigma_y \sigma_z} \exp\left(-\frac{y^2}{2\sigma_y^2} - \frac{z^2}{2\sigma_z^2}\right) \tag{1}$$

where y and z are the transverse and vertical directions, with the source located at $y = z = 0$, σ_y and σ_z are the standard deviations of the transverse and vertical distributions of concentration, Q is the release rate, and U is the mean wind speed across the plume.

The transverse dispersion coefficient σ_y is calculated using Taylor's (1921) theory, assuming horizontally homogeneous turbulence. The turbulent diffusion analysis of Taylor (1921) predicts linear plume growth for $t < T_L$ (i.e., in the near field), where T_L is the Lagrangian time scale, and parabolic growth for $t > T_L$ (i.e., in the far field). The far-field parabolic formulation corresponds to the configuration of a plume larger than the turbulence length scale. Inside the canopy the turbulence length scales are comparable to the height of the buildings and the widths of the canyons. Since in this study we focus on the near-field dispersion below the canopy height, the plume does not grow larger than the turbulence length scales, and only the near-field approximation of Taylor's relation is needed:

$$\sigma_y^2 = \sigma_{yo}^2 + \sigma_v^2 t^2 \tag{2}$$

where σ_{yo} is the plume transverse standard deviation at the source, and σ_v is the standard deviation of the Lagrangian transverse velocity v.

The vertical dispersion coefficient σ_z is defined using the approach of Hunt and Weber (1979) for ground-level sources in the neutral atmosphere.

$$\sigma_z^2 = \sigma_{zo}^2 + b^2 \sigma_w^2 t^2 \tag{3}$$

where σ_{zo} is the plume vertical standard deviation at the source, and b is an empirical constant. Franzese and Huq (2011) used $b = 1$ for daytime atmosphere, and $b = 0.5$ for nighttime atmosphere; the value $b = 1$ is used in this study.

The values of σ_v, σ_w, and U used in the model have been calculated as follows:

1. Equation 2 is written as $\sigma_y^2 = \sigma_{yo}^2 + (\sigma_v/U)^2 x^2$, and the ratio σ_v/U is obtained by a best fit to the experimental data of σ_y, which are measured at different distances x.
2. The relationship $\sigma_w = 2/3\sigma_v$ is assumed, and Eq. 3 is written as $\sigma_z^2 = \sigma_{zo}^2 + 4/9b^2(\sigma_v/U)^2 x^2$. The assumption $\sigma_w = 2/3\sigma_v$ was used in Franzese and Huq (2011), and is in accord with field measurements reported by Roth (2000) and Hanna et al. (2007), and with laboratory measurements by Cheng and Castro (2002).
3. Finally, U is estimated by a best fit of Eq. 1 to the observed concentrations. The values of σ_v, σ_w, and U are now determined.

4 Mean Velocity and Turbulence Measurements

Here we present plots of experimental measurements of mean velocity, turbulent fluctuations and Reynolds stress for $A_r = 1$ and $A_r = 3$ taken at the centreline of the canyon, at $x/B = 38$. The data for $A_r = 0.25$ are available in Macdonald and Ejim (2002), but are not reported here as they are spatially averaged and are not directly comparable.

4.1 Mean Velocity

Vertical profiles of the non-dimensional mean velocity U/U_∞ for both the $A_r = 1$ and $A_r = 3$ canopies are presented in Fig. 2. The mean velocity at the building height is $U_b = 52$ mm

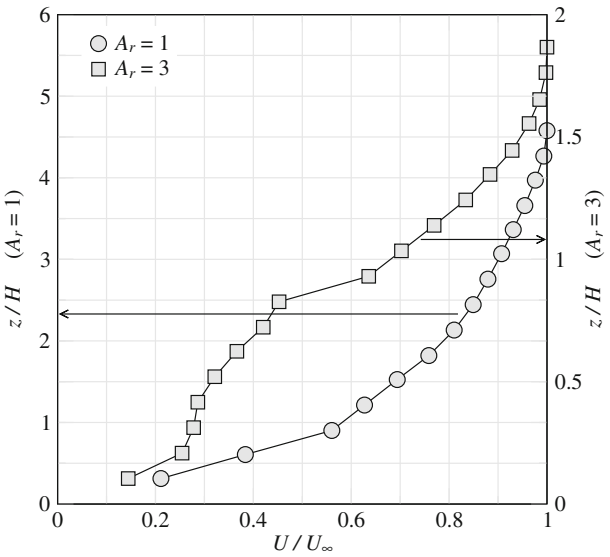

Fig. 2 Vertical profiles of the non-dimensional alongwind mean velocity U/U_∞ for the $A_r = 1$ and the $A_r = 3$ canopies. The ordinate on the left is for $A_r = 1$ and the ordinate on the right is for $A_r = 3$

$s^{-1}(U_b \approx 0.6U_\infty)$ for $A_r = 1$, and $U_b = 77\,\text{mm}\ s^{-1}(U_b \approx 0.7U_\infty)$ for $A_r = 3$. Near ground level, at about $H/6$, velocities are approximately one third of the rooftop velocity for both canopies.

For the short canopy, the large velocity gradients in the vicinity of the rooftop level and the ground indicate the presence of shear layers. The profile has a power-law like growth, with no inflection. The measurements of Macdonald et al. (2000) for a short canopy display the variation of the form of the velocity profile as a function of the lateral position, and show that vertical profiles behind a building possess a pronounced inflection, whereas the profiles in the canyon do not. Thus our profile does not exhibit an inflection point at rooftop level because it was measured at the centreline of the canyon.

For the tall canopy the velocity profile shows slow growth with height up to the rooftop level, where there is an inflection point, and a power-law growth above. A possible explanation for the form of the profile including an inflection point may be related to the larger area factor of the tall canopy ($\lambda_f = 0.56$). The turbulent wakes behind the buildings of the tall canopy are very anisotropic, with a vertical length scale about three times the horizontal length scale. Since the buildings are relatively close to each other ($G = H/3$), and the wind speed at the rooftop level is relatively high, the wake may extend or fluctuate laterally and reach the canyon centreline. Therefore, the velocity profile at the canyon centreline for a tall canopy displays a signature of the wake, namely an inflection point.

4.2 Velocity Fluctuations

Vertical profiles of the non-dimensional r.m.s. of longitudinal velocity σ_u/U_∞ are plotted in Fig. 3. The values of σ_u for both canopies have a peak in excess of $0.1U_\infty$ slightly below the rooftop level, and decrease to background values ($\sigma_u \approx 0.055U_\infty$) aloft. Within the canopy, σ_u is relatively constant ($\approx 0.1U_\infty$) for the short canopy, while for the tall canopy it increases with height, with values at rooftop level about twice as large as at ground level. The different

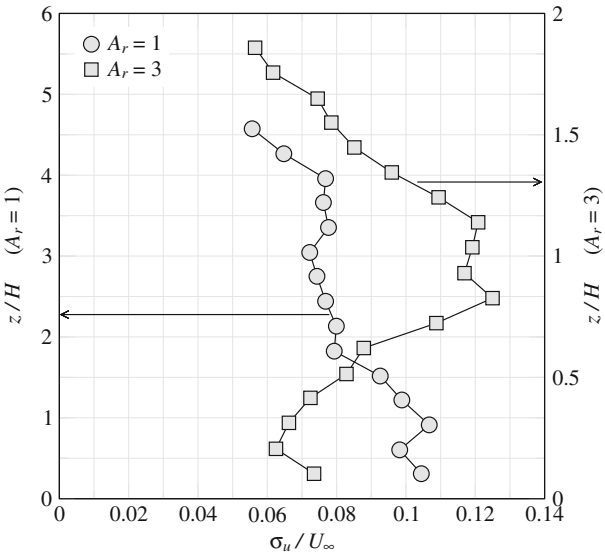

Fig. 3 Vertical profiles of the non-dimensional alongwind velocity fluctuation σ_u/U_∞ for the $A_r = 1$ and the $A_r = 3$ canopies

behaviour of σ_u near the ground between the two canopies arises from the presence of the wake at the canyon centreline for the $A_r = 3$ canopy. In contrast, the wake does not extend to the canyon centreline for the $A_r = 1$ canopy, consistent with the features of the mean wind profile in Fig. 2 and its related discussion. Near ground level, for both canopies $\sigma_u \approx 0.5U$, where U is the local mean flow speed, in agreement with field data for Oklahoma City and New York City (Hanna et al. 2007).

Figure 4 shows the profiles of the non-dimensional r.m.s. of vertical velocity σ_w/U_∞. The profiles display a region of enhanced turbulence intensity near the rooftop level, and the peak values of σ_w also occurring slightly below the rooftop level.

4.3 Reynolds Stress

The vertical profiles of the non-dimensional Reynolds stress $-\overline{uw}/U_\infty^2$ are presented in Fig. 5. The Reynolds stress is negative at the ground and up to about 0.3–0.5 of the canopy height. The negative values near the ground may not have a clear physical interpretation, because they are small (about one order of magnitude smaller than at the rooftop level) and the uncertainty associated with the Reynolds stress is larger than for the turbulent velocity variances. The negative Reynolds stress near the ground can easily be the result of experimental errors. Small negative values are also found in the wind-tunnel measurements of Castro et al. (2006) for cube arrays, and of Kastner-Klein and Rotach (2004) for a scale model city of Nantes, France.

In the vicinity of the rooftop level the signature of a shear layer is evident in the elevated values of the Reynolds stress profiles. The vertical extent of the shear layer is about $2H$ for the short canopy and H for the tall canopy, in agreement with the analysis of Huq et al. (2007). Above the rooftop level, the non-monotonic behaviour may be partially due to experimental error, although other factors such as turbulence inhomogeneities due to the vortex generator may have played a role.

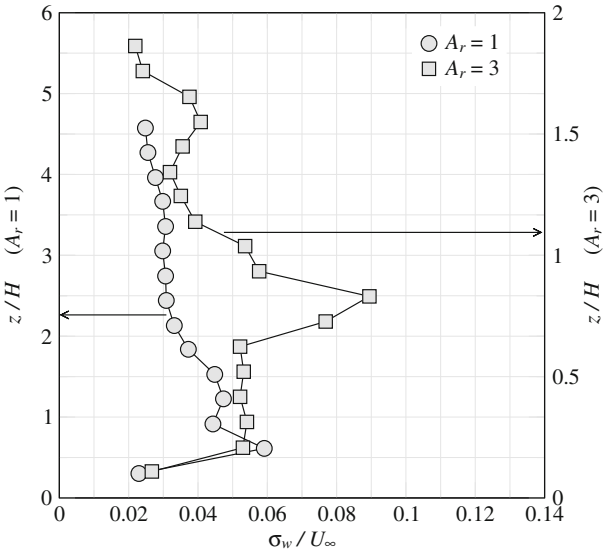

Fig. 4 Vertical profiles of the non-dimensional vertical velocity fluctuation σ_w/U_∞ for the $A_r = 1$ and the $A_r = 3$ canopies

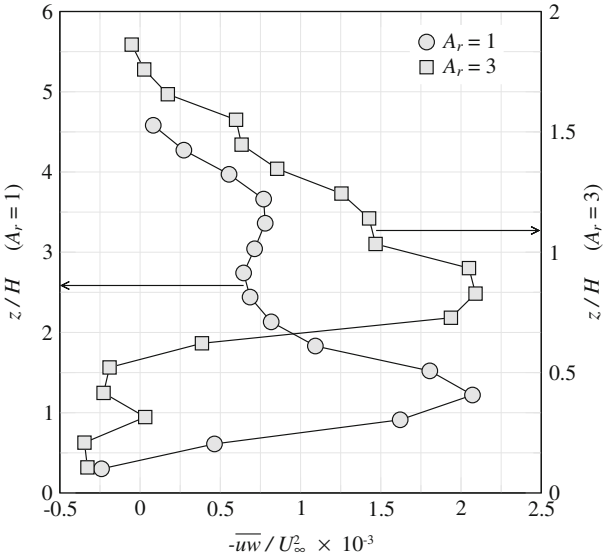

Fig. 5 Vertical profiles of the non-dimensional Reynolds stress $-\overline{uw}/U_\infty^2$ for the $A_r = 1$ and the $A_r = 3$ canopies

In summary, the profiles of mean velocity, turbulent fluctuations and Reynolds stress suggest four different turbulence regimes within the canopy flow:

1. *Near the ground*—the Reynolds stress is comparable for both canopies. A shear layer develops as the large mean velocity gradient dU/dz energizes turbulence production $-\overline{uw}dU/dz$. The vertical fluctuations are weaker than the horizontal fluctuations

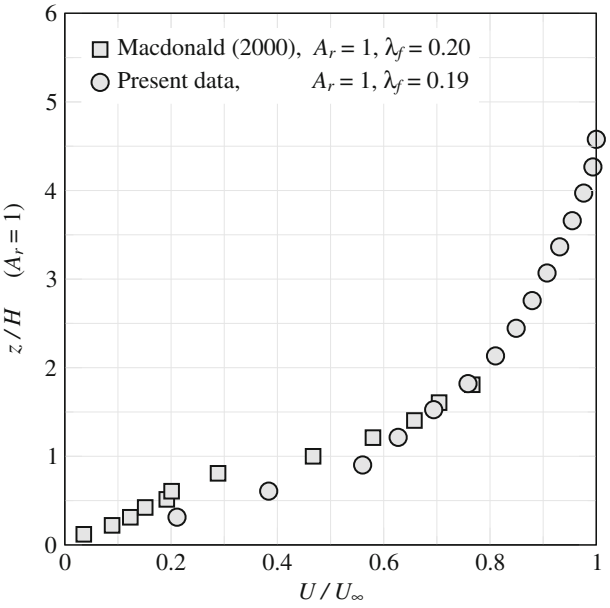

Fig. 6 Comparison of the wind-speed profiles for the $A_r = 1$ canopy with the wind-tunnel measurements reported by Macdonald (2000)

because of the attenuating effect of the ground. The magnitude of σ_u is larger for the short canopy mainly because the near-ground wind speed for the short canopy is larger than for the tall canopy. This is consistent with the observed $\sigma_u/U \approx 0.5$ for both canopies, where U is the local mean wind speed. In addition, σ_u for the short canopy may be enhanced by the rooftop shear layer which extends downward to the ground, in contrast with the shear layer from a tall canopy, which does not (Huq et al. 2007).

2. *Mid-height*—in the short canopy, the higher wind speeds enhance the horizontal turbulent fluctuations. The shear layer from the rooftop of the short canopy may also contribute to the production of turbulence (the shear layer from the tall canopy may not reach down to mid-height). As a consequence, the tall canopy displays weaker levels of horizontal turbulence.
3. *Rooftop level*—the dynamics are dominated by the shear layer, which results in large values of Reynolds stress, horizontal and vertical turbulent fluctuations.
4. *Above the canopy*—turbulence gradually attenuates to the background levels aloft.

4.4 Comparisons with Other Data

Figure 6 shows a comparison of the present wind-speed profiles with the wind-tunnel measurements over regular arrays of cubic obstacles reported by Macdonald (Hall et al. 2000; see also 1998) for a comparable value of $\lambda_f = 0.2$. Within the canopy the flow is laterally inhomogeneous because of the alternance of buildings and canyons. The data of Macdonald (2000) are laterally averaged between the wake and the canyon whereas our measurements are taken at the canyon centreline. This leads to two differences between the datasets, namely the values of Macdonald (2000): (i) possess an inflection point; and (ii) are smaller within the canopy, as flow speeds in the wake are smaller than in the canyon. Above the canopy,

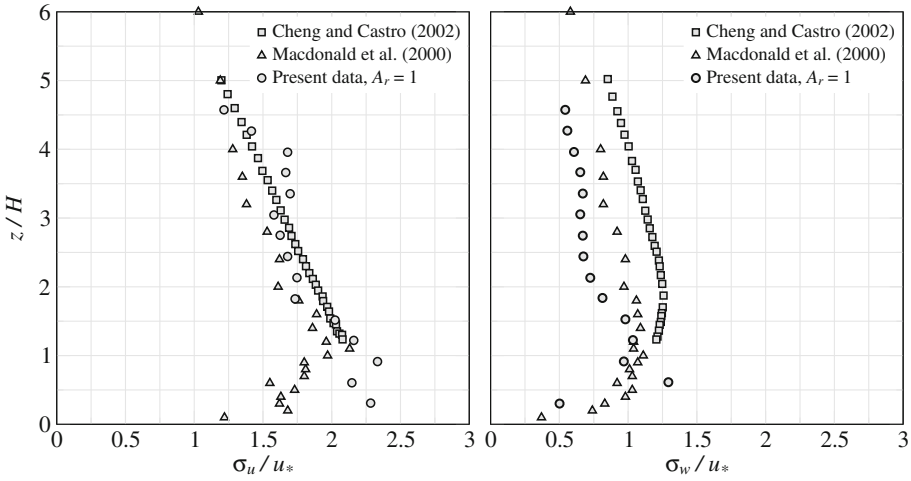

Fig. 7 Comparison of σ_u/u_* and σ_w/u_* profiles for the $A_r = 1$ canopy with the wind-tunnel measurements reported by Cheng and Castro (2002) and by Macdonald et al. (2000)

where the influence of the wakes and the canyons are small, the two datasets are in better agreement.

The turbulence measurements normalized by the friction velocity u_* compare well with field data in urban areas reported by Hanna et al. (2007). In our experiments u_* was estimated as the square root of the peak value of the Reynolds stress; $u_* = 4.3\,\text{mm s}^{-1}$ for $A_r = 1$, and $u_* = 5\,\text{mm}\,s^{-1}$ for $A_r = 3$. In Oklahoma City ($A_r \approx 1$) at a height of 8 m $\sigma_w/u_* = 1.5$, compared to our measured $\sigma_w/u_* = 1.3$ at the rooftop level; in Manhattan ($A_r \approx 3$), $\sigma_w/u_* = 1.8$ at the rooftop level, compared to our measured $\sigma_w/u_* = 2$.

Our rooftop values for σ_u are also in good agreement with field data: in Oklahoma City $\sigma_u/u_* = 2.4$ at 8 m, which compares to our measured $\sigma_u/u_* = 2.3$ at the rooftop level. In Manhattan the observed $\sigma_u/u_* = 2.4$ at the rooftop level, which compares to our measured $\sigma_u/u_* = 2.7$.

Typical values of turbulence intensities for a neutral boundary layer are $\sigma_w/u_* \approx 1.3$ and $\sigma_u/u_* \approx 2.5$. Thus the results suggest that for short canopies the rooftop values of σ_w/u_* and σ_u/u_* are comparable to the values for a neutral boundary layer. For tall canopies, horizontal turbulent intensity is comparable, but the vertical turbulence intensity is higher than for the neutral boundary layer. This suggests that the neutral boundary-layer similarity scaling may not apply to tall canopies, or may require different values of turbulence intensities.

Figure 7 shows a comparison of the present data for σ_u and σ_w normalized by u_* with the measurements taken by Cheng and Castro (2002) for arrays with $\lambda_f = 0.25$ and by Macdonald et al. (2000) for arrays with $\lambda_f = 0.16$. Note that the array used in Cheng and Castro (2002) differs from the others in that it is aligned in the longitudinal direction but not in the crosswind direction. The values of σ_u/u_* are all in good agreement above the rooftop level. Within the canopy, our values do not decrease as do those of Macdonald et al. (2000) because our measurements are taken at the canyon centreline, whereas those of Macdonald et al. (2000) are laterally averaged. Our σ_w/u_* data values above the canopy are typically about 50 % of the Cheng and Castro (2002) values and about 75 % of the Macdonald et al. (2000) values. A notable difference is the location of our peak below the rooftop level.

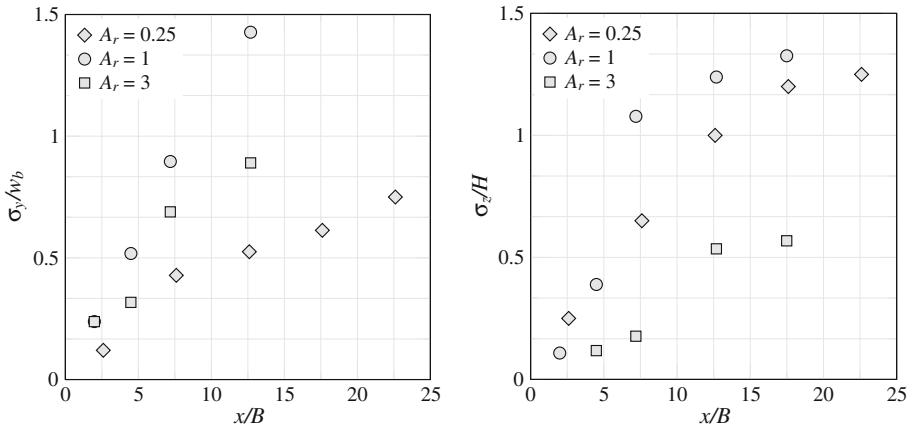

Fig. 8 Downwind evolution of the normalized transverse spread σ_y/w_b (*left panel*) and vertical spread σ_z/H (*right panel*) as functions of normalized distance from the source x/B

Several factors contribute to the differences between the experimental values of the datasets, including: (i) the method of accelerating boundary-layer development (e.g., the presence or absence of a vortex generator); (ii) instrument resolution; (iii) inertial effects of the particles used for the PIV measurements; (iv) downwind measurement location (i.e., the fetch); (v) spatial averaging of measurements; and (vi) different experimental configurations (such as different area factors, or alignment of the arrays in the longitudinal but not in the crosswind directions).

5 Dispersion and Model Comparison

Above the canopy, dispersion is mainly determined by the background turbulence characteristics of the atmospheric boundary layer (Franzese and Huq 2011). In contrast, dispersion below the canopy is determined by a number of factors including the configuration of the buildings and the location of the source. For instance, the relevant turbulence time and length scales controlling dispersion are related to the mean building height and to the spacing between buildings. In this section we present the observed plume spreads and concentration data for the $A_r = 0.25$, 1 and 3 canopies. Using appropriate scales, the data for all canopies can be non-dimensionalized, represented together in the same plot, and compared with the model predictions.

5.1 Plume Spreads

The measurements of plume transverse and vertical spreads σ_y and σ_z were obtained by fitting the transverse and vertical profiles of concentration with Gaussian and reflected Gaussian relations, respectively. The concentration profiles were Gaussian to a good approximation, ensuring a satisfactory fit. Figure 8 shows the evolution of the measured σ_y/w_b and σ_z/H as functions of downwind distance x/B from the source. The data for σ_y/w_b and σ_z/H do not vary systematically with aspect ratio, nor do the data collapse, suggesting that other scales besides B, w_b and H influence dispersion. For instance, advection needs to be explicitly included, because the experiments were conducted using different freestream velocities.

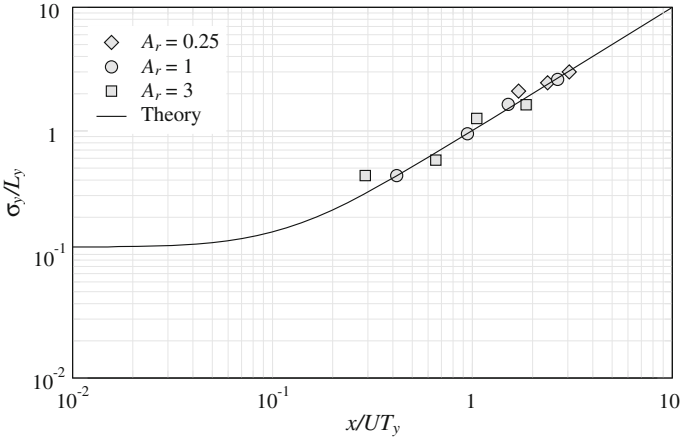

Fig. 9 Growth rate of σ_y/L_y as a function of the non-dimensional distance x/UT_y, along with the prediction of Eq. 2

In order to perform a meaningful comparison between model results and canopies with different aspect ratios, the measurements are scaled by the transverse and vertical turbulence length scales L_y and L_z, the transverse and vertical turbulence time scales T_y and T_z, and the advection velocity U. The data are represented as σ_y/L_y versus x/UT_y, and σ_z/L_z versus x/UT_z, noting that physically x/UT_y and x/UT_z are ratios of advective to overturning time scales. Within the urban canopy, H is a natural choice for the vertical length scale of the turbulence, hence we assume $L_z = H$. Likewise, the width of the canyon G (see Fig. 1) can be associated with the transverse size of the largest eddies between the buildings. Because eddies are shed from the buildings on both sides of the gap, the transverse length scale for the turbulence can be taken as $L_y = G/2$. The measurements of velocity correlations in the experiments of Castro et al. (2006) for above-canopy turbulence show that L_z tends to H and L_y tends to $H/2$ as z tends to H from above. Since $G = H$ in the canopy used by Castro et al. (2006), their measured L_y is consistent with our assumption $L_y = G/2$. The turbulence time scales are estimated as $T_y = L_y/\sigma_v$ and $T_z = L_z/\sigma_w$.

Equation 1 was derived for ground-level sources. Since the source for the $A_r = 0.25$ canopy was located at the mid-height of the buildings, the maximum concentration near the source does not occur at the ground. At larger distances, the effect of the source height becomes negligible. Therefore, the data for $A_r = 0.25$ at the two closest distances $x/B = 0.26$ and 7.6 are not included in our comparisons. Values of quantities used in the model and for scaling the data are summarized in Table 1. The choice of σ_v and U was determined through the fitting procedure described in Sect. 3: U is a characteristic value of the velocity profile over the height of the plume (i.e., over σ_z for ground-level releases). As the aspect ratio increases, the distance from the rooftop level to the centre of the plume increases and thus U/U_b varies inversely with the aspect ratio. Note that for the $A_r = 0.25$ canopy $U = U_b$ because the plume is modelled only at the far downwind stations, where $\sigma_z \approx H$, as shown in Fig. 8. As a general rule, we obtained $\sigma_v/U \approx 0.1$ for the three canopies. Figure 9 shows the growth rate of σ_y/L_y as a function of the non-dimensional distance x/UT_y, along with the prediction of Eq. 2. The non-dimensional data for all canopies collapse well and follow a linear plume growth in accord with Eq. 2; the curve approaches the source size σ_o/L_y as $x \to 0$.

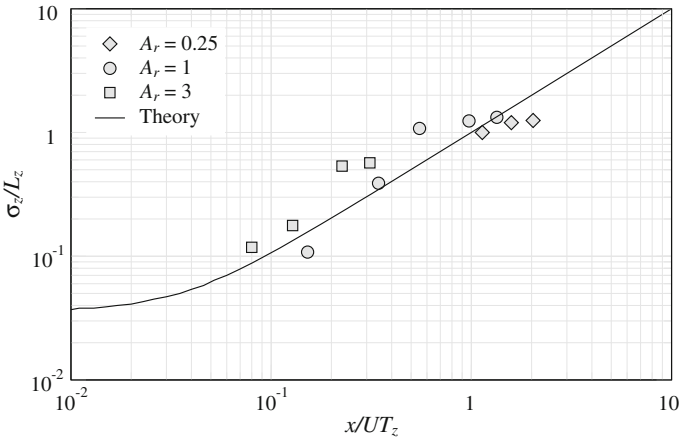

Fig. 10 Growth rate of σ_z/L_z as a function of the non-dimensional distance x/UT_z, along with the prediction of Eq. 3

The laboratory data for the downwind evolution of σ_z/L_z along with the theoretical prediction given by Eq. 3 are shown in Fig. 10. The model compares well with the data, although the scatter for σ_z is larger compared to σ_y, due to the limited vertical extent of the measurements, and possibly to the approximation introduced by the assumption $\sigma_w = 2/3\sigma_v$.

5.2 Concentration

Figure 11 shows the downwind evolution of vertical profiles of normalized centreline concentration C/C_o, where C_o is the concentration at the source, for the three urban canopies. For the $A_r = 0.25$ canopy the effect of the source height (at $z = 0.5H$) on the form of the profile and on the location of the peak concentration becomes negligible after $x/H = 12.6$. For $A_r = 1$ the vertical profiles have a maximum at the ground and strong vertical gradients at short distances from the source. The profiles become nearly uniform after $x/B > 7.5$. Vertical gradients near the source are also large for $A_r = 3$ but the profiles do not become vertically uniform even at the furthest station at $x/B = 17.8$. The differences between modelled and observed vertical profiles at short distances arise from the approximations inherent in the model, namely the use of a unique U at all distances, and the use of analytical relations (as opposed to measured values) for σ_y and σ_z. An additional approximation is introduced by the effects of the non-zero source momentum flux at short distances, which are not accounted for by the model. Figure 12 shows the good agreement between C/C_o at ground level predicted by Eq. 1 and the measurements for all canopy experiments.

The evolution of the measured concentration data, non-dimensionalized as CUL_yL_z/Q, with the scaled distance from the source x/UT, where $T = (T_yT_z)^{1/2}$, are plotted in Fig. 13. The data for all three canopies collapse well, and follow the $C \sim x^{-2}$ decay predicted by Eq. 1. The decay can be described by the relation $CUL_yL_z/Q = (kU^2T^2)x^{-2}$ with $k \approx 0.3$. The advantage of using the non-dimensional group CUL_yL_z/Q compared to other groups such as, e.g., CU/Q, is that the latter does not account for the geometry of the canopy, therefore it may not collapse the data from canopies with different aspect ratios.

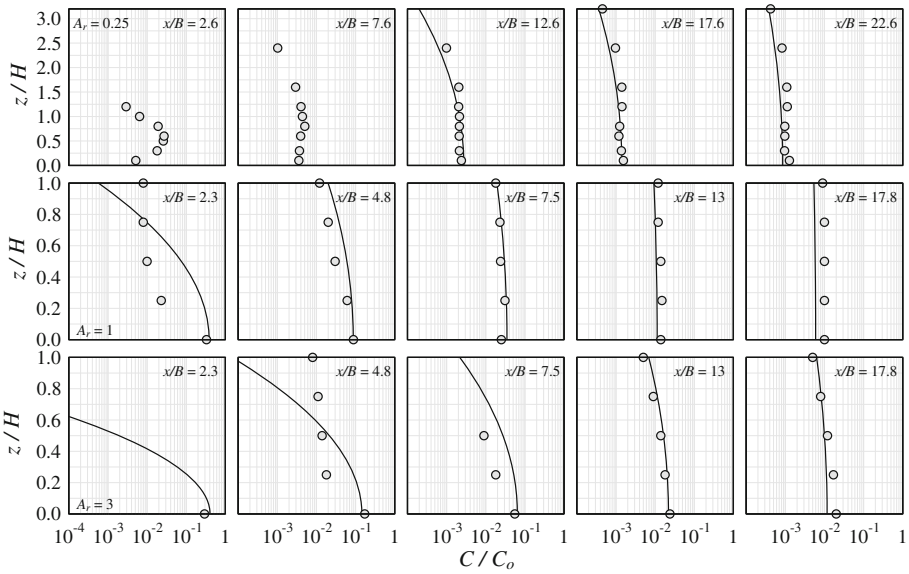

Fig. 11 Vertical profiles of normalized mean concentration C/C_o, where C_o is the concentration at the source, at various distances from the source x/B at the plume centreline. The solid lines are the reflected Gaussian profile of Eq. 1

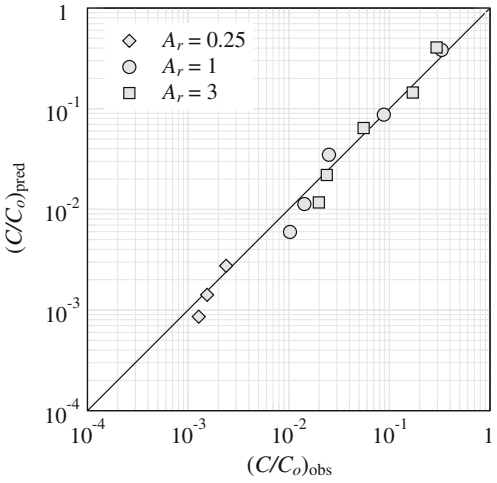

Fig. 12 Predicted versus observed normalized ground-level concentration C/C_o

The non-dimensional groups CUL_yL_z/Q and x/UT both include the variables U and T because CUL_yL_z/Q can be written as $CU\sigma_v\sigma_wT^2/Q$. Therefore, it is possible that the observed relationship between CUL_yL_z/Q and x/UT is partially spurious. The amount of spurious correlation arising from the common variables U and T was examined in detail in Franzese and Huq (2011) for urban dispersion data from field experiments and found to be negligible.

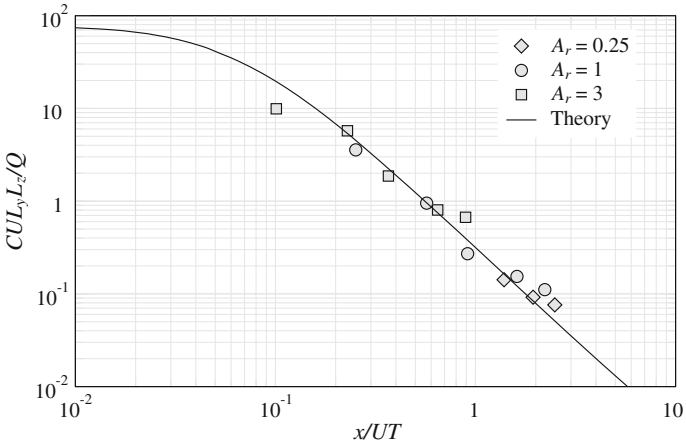

Fig. 13 Measured non-dimensional concentration CUL_yL_z/Q as a function of the non-dimensional distance from the source x/UT, along with the model prediction of Eq. 1

6 Conclusions

We presented water-tunnel measurements of velocity, turbulence, and concentration for three different model urban canopies. The measurements for the canopy with aspect ratio of building height to width $A_r = 0.25$ were taken by Macdonald and Ejim (2002); the data for the canopies with $A_r = 1$ and 3 are new. The direction of the mean flow was parallel to the canyons, a passive scalar was continuously released from a point source, and concentration was measured at different distances from the source and at different heights above the ground. The observed plume transverse and vertical spreads were compared with analytical relations derived from the theories of Taylor (1921) and Hunt and Weber (1979), which predict linear growth in both the transverse and vertical directions. The concentration data were compared with the predictions of a Gaussian model, which predicts a -2 power-law decay of concentration with distance from the source.

Spreads, concentrations and distance from the source were non-dimensionalized using L_y, L_z, T_y, T_z, and U, which were defined based on the geometry of the buildings. Such scaling collapses the data for all three aspect ratios, and is valid as long as $\sigma_z \leqslant H$. An estimate of distances for which the plume remains below the canopy height H can be obtained from the σ_z data reported in Fig. 10, which show that $\sigma_z \approx L_z$ at $x \approx UT_z$. Using the typical urban canopy values $L_z = 20\,\text{m}$, $U = 3$–$5\,\text{m s}^{-1}$ and $\sigma_w = 0.7\,\text{m s}^{-1}$, the plume remains below the canopy up to a distance of approximately 100 m from the source; for larger distances the scaling is determined by characteristics of the atmospheric turbulence above the canopy (Franzese and Huq 2011). In all experiments the source was located at the centreline of the canyon. For sources located behind a building the dynamics of dispersion is affected by the recirculating region in the building wake. In this case, the model accuracy may be improved by explicitly including the source effects (e.g., by using a virtual source size).

The wind direction in the experiments was parallel to the direction of the canyons. Small variations of wind direction have a negligible effect as the plume maintains its alignment with the axis of the canyon because of alongwind channelling of the flow. Wind directions at large angles to the canyon centreline would alter the frontal area density, the wind-speed and turbulence profiles, and would cause plume veering due to crosswind channelling of the flow.

Acknowledgements This work was initiated while P.F. was affiliated with George Mason University. This material is partly based upon work supported by the National Science Foundation under Grants AGS 0849190 and 0849191.

References

Biltoft CA (2001) Customer report for Mock Urban Setting Test. Tech. Rep. WDTC-FR-01-121, U.S. Army Dugway Proving Ground, Dugway, Utah

Castro IP, Robins AG (1977) The flow around a surface-mounted cube in uniform and turbulent streams. J Fluid Mech 79: 307–335

Castro IP, Cheng H, Reynolds R (2006) Turbulence over urban-type roughness: deductions from wind-tunnel measurements. Boundary-Layer Meteorol 118(1): 109–131

Cheah SC, Cleaver JW, Millward A (1983) Water channel simulation of the atmospheric boundary layer. Atmos Environ 17(8): 1439–1448

Cheng H, Castro IP (2002) Near wall flow over urban-like roughness. Boundary-Layer Meteorol 104(2): 229–259

Chin HNS, Leach MJ, Sugiyama GA, Leone JM, Walker H, Nasstrom JS, Brown MJ (2005) Evaluation of an urban canopy parameterization in a mesoscale model using VTMX and URBAN 2000 data. Mon Weather Rev 133(7): 2043–2068

Coceal O, Thomas T, Castro IP, Belcher S (2006) Mean flow and turbulence statistics over groups of urban-like cubical obstacles. Boundary-Layer Meteorol 121: 491–519

Collier CG (2006) The impact of urban areas on weather. Q J R Meteorol Soc 132(614): 1–25

Counihan J (1969) An improved method of simulating an atmospheric boundary layer in a wind tunnel. Atmos Environ 3(2): 197–200

Delle Monache L, Weil J, Simpson M, Leach MJ (2009) A new urban boundary layer and dispersion parameterization for an emergency response modeling system: Tests with the Joint Urban 2003 data set. Atmos Environ 43: 5807–5821

Dobre A, Arnold SJ, Smalley RJ, Boddy JWD, Barlow JF, Tomlin AS, Belcher SE (2005) Flow field measurements in the proximity of an urban intersection in London, UK. Atmos Environ 39(26): 4647–4657

Franzese P, Huq P (2011) Urban dispersion modelling and experiments in the daytime and nighttime atmosphere. Boundary-Layer Meteorol 139: 395–409

Gailis RM, Hill A (2006) A wind-tunnel simulation of plume dispersion within a large array of obstacles. Boundary-Layer Meteorol 119(2): 289–338

Golden J (1961) Scale model techniques. Master's thesis, College of Engr., New York Univ., New York, 48 pp

Grimmond CSB, Oke TR (1999) Aerodynamic properties of urban areas derived from analysis of surface form. J Appl Meteorol 38(9): 1262–1292

Grimmond CSB, Salmond JA, Oke TR, Offerle B, Lemonsu A (2004) Flux and turbulence measurements at a densely built-up site in Marseille: Heat, mass (water and carbon dioxide), and momentum. J Geophys Res 109, D24101, D24, p 19

Hall DJ, Macdonald RW, Walker S, Spanton AM (1998) Measurements of dispersion within simulated urban arrays: a small scale wind tunnel study. Tech. Rep. CR 244/98, Building Research Establishment

Hanna SR, Britter RE, Franzese P (2003) A baseline urban dispersion model evaluated with Salt Lake City and Los Angeles tracer data. Atmos Environ 37(36): 5069–5082

Hanna SR, White J, Zhou Y (2007) Observed winds, turbulence, and dispersion in built-up downtown areas of Oklahoma City and Manhattan. Boundary-Layer Meteorol 125(3): 441–468

Hunt JCR, Weber AH (1979) A Lagrangian statistical analysis of diffusion from a ground-level source in a turbulent boundary layer. Q J R Meteorol Soc 105(444): 423–443

Huq P (1997) Observations of jets in density stratified crossflows. Atmos Environ 31(13): 2011–2022

Huq P, Carrillo A, White LA, Redondo J, Dharmavaram S, Hanna SR (2007) The shear layer above and in urban canopies. J Appl Met Climatol 46(3): 368–376

Kastner-Klein P, Rotach MW (2004) Mean flow and turbulence characteristics in an urban roughness sublayer. Boundary-Layer Meteorol 111(1): 55–84

Luhar AK, Venkatram A, Lee SM (2006) On relationships between urban and rural near-surface meteorology for diffusion applications. Atmos Environ 40(34): 6541–6553

Macdonald RW (2000) Modelling the mean velocity profile in the urban canopy layer. Boundary-Layer Meteorol 97(1): 25–45

Macdonald RW, Ejim CE (2002) Flow and dispersion data from a hydraulic simulation of the MUST array. Thermal Fluids Report 2002–2003, University of Waterloo, Waterloo

Macdonald RW, Griffiths RF, Hall DJ (1998) An improved method for the estimation of surface roughness of obstacle arrays. Atmos Environ 32(11): 1857–1864

Macdonald RW, Carter S, Slawson PR (2000) Measurements of mean velocity and turbulence statistics in simple obstacle arrays at 1:200 scale. Thermal Fluids Report 2000-1, Department of Mechanical Engineering, University of Waterloo, Waterloo

Mestayer PG, Durand P, Augustin P, Bastin S, Bonnefond JM, Bénech B, Campistron B, Coppalle A, Delbarre H, Dousset B, Drobinski P, Druilhet A, Fréjafon E, Grimmond CSB, Groleau D, Irvine M, Kergomard C, Kermadi S, Lagouarde JP, Lemonsu A, Lohou F, Long N, Masson V, Moppert C, Noilhan J, Offerle B, Oke TR, Pigeon G, Puygrenier V, Roberts S, Rosant JM, Saïd F, Salmond J, Talbaut M, Voogt J (2005) The urban boundary-layer field campaign in Marseille (UBL/CLU-ESCOMPTE): set-up and first results. Boundary-Layer Meteorol 114: 315–365

Milliez M, Carissimo B (2007) Numerical simulations of pollutant dispersion in an idealized urban area, for different meteorological conditions. Boundary-Layer Meteorol 122(2): 321–342

Molina MJ, Molina LT (2004) Megacities and atmospheric pollution. J Air Waste Manag Assoc 54(6): 644–680

Oke TR (1987) Boundary layer climates. Routledge, 460 pp

Rajaratnam N (1976) Turbulent jets. Elsevier Science Ltd, Amsterdam 304 pp

Rotach MW (1995) Profiles of turbulence statistics in and above an urban canyon. Atmos Environ 29(13): 1473–1486

Rotach MW, Vogt R, Bernhofer C, Batchvarova E, Christen A, Clappier A, Feddersen B, Gryning SE, Martucci G, Mayer H, Mitev V, Oke TR, Parlow E, Richner H, Roth M, Roulet YA, Ruffieux D, Salmond JA, Schatzmann M, Voogt JA (2005) BUBBLE: an urban boundary layer meteorology project. Theor Appl Climatol 81(3–4): 231–261

Roth M (2000) Review of atmospheric turbulence over cities. Q J R Meteorol Soc 126(564): 941–990

Schlichting H (1968) Boundary layer theory. McGraw-Hill, New York, 747 pp

Snyder WH (1981) Guideline for fluid modeling of atmospheric diffusion. Tech. Rep. EPA-600/8-81-009, U.S. Environmental Protections Agency, Research Triangle Park, North Carolina, 185 pp

Snyder WH, Castro IP (2002) The critical Reynolds number for rough-wall boundary layers. J Wind Eng Ind Aerodyn 90(1): 41–54

Taylor GI (1921) Diffusion by continuous movements. Proc Lond Math Soc 20: 196–211

Yee E, Gailis RM, Hill A, Hilderman T, Kiel D (2006) Comparison of wind-tunnel and water-channel simulations of plume dispersion through a large array of obstacles with a scaled field experiment. Boundary-Layer Meteorol 121(3): 389–432